micromachines

MDPI

Article

Silicon Wafer Etching Rate Characteristics with Burst Width Using 150 kHz Band High-Power Burst Inductively Coupled Plasma

Hisaki Kikuchi [1], Katsuyuki Takahashi [1,2], Seiji Mukaigawa [1], Koichi Takaki [1,2,*] and Ken Yukimura [1]

[1] Department of Systems Innovation Engineering, Faculty of Science and Engineering, Iwate University, Morioka, Iwate 020-8551, Japan; g0320041@iwate-u.ac.jp (H.K.); ktaka@iwate-u.ac.jp (K.T.); mukaigaw@iwate-u.ac.jp (S.M.); keny@gaia.eonet.ne.jp (K.Y.)

[2] Agri-Innovation Center, Iwate University, Morioka, Iwate 020-8550, Japan

* Correspondence: takaki@iwate-u.ac.jp; Tel.: +81-19-621-6460

Abstract: The high-speed etching of a silicon wafer was experimentally investigated, focusing on the duty factor of 150 kHz band high-power burst inductively coupled plasma. The pulse burst width was varied in the range of 400–1000 μs and the repetition rate was set to 10 Hz. A mixture of argon (Ar) and carbon tetrafluoride (CF_4) gas was used as the etching gas and injected into the vacuum chamber. The impedance was changed with time, and the coil voltage and current were changed to follow it. During the discharge, about 3 kW of power was applied. The electron temperature and plasma density were measured by the double probe method. The plasma density in the etching region was 10^{18}–10^{19} m^{-3}. The target current increased with t burst width. The etching rate of Ar discharge at burst width of 1000 μs was 0.005 μm/min. Adding CF_4 into Ar, the etching rate became 0.05 μm/min, which was about 10 times higher. The etching rate increased with burst width.

Keywords: ICP; etching; HiPIMS; high power; burst pulse; double probe measurement; CF_4; Ar

Citation: Kikuchi, H.; Takahashi, K.; Mukaigawa, S.; Takaki, K.; Yukimura, K. Silicon Wafer Etching Rate Characteristics with Burst Width Using 150 kHz Band High-Power Burst Inductively Coupled Plasma. *Micromachines* **2021**, *12*, 599. https://doi.org/10.3390/mi12060599

Academic Editors: Lucia Romano and Konstantins Jefimovs

Received: 30 April 2021
Accepted: 20 May 2021
Published: 22 May 2021

1. Introduction

Plasma processing, a material processing technique using plasma, is an essential part of today's manufacturing industries. Plasma-based surface processes are used to manufacture micro and nano order high-density integrated circuits for the electronics industry, specifically, for plasma etching to remove unnecessary parts of the circuit substrate and for sputtering to form thin metal films in the semiconductor device manufacturing process [1–3]. Plasma etching is used in processes such as patterning, planarization, removal of damaged layers, and resist removal (ashing). Nowadays, ultrafine processing techniques are required to meet the demand for large-scale integrated circuits, and a high-density plasma source is necessary to achieve this [4]. Inductively coupled plasma (ICP) has been widely used as a plasma source because of its advantages, such as simple equipment configuration and high density plasma at low pressure [5–9]. ICP can be generated with electrodeless electrodes, and the positive ions can be independently controlled by the bias voltage applied to the substrate [5–8,10].

A new ICP system using burst waves has been developed [11–17]. In this system, the frequency is set to 100–200 kHz, which is not necessary for the impedance matching circuit required in conventional ICP systems, and the resonance between the ICP inductance and the parallel capacitance produces high-density plasma of the order of 10^{19} m^{-3} [12–17]. Therefore, this ICP system has the advantage of a simple equipment configuration. In fact, the plasma source is compact, with a cylindrical shape and about 50 mm in diameter, which costs less than conventional systems. In addition, the burst width and duty ratio can be freely set to optimize the process conditions. This plasma source can also be installed in a minimal fab system that processes half-inch wafers to produce semiconductor devices [18,19].

In this study, reactive ion etching was performed using a tetrafluoro-carbon (CF_4) and argon (Ar) mixed gas atmosphere, and the etching rate was compared with that of physical etching using argon gas atmosphere. It has been reported that the etching rate of the burst wave ICP is affected by the substrate bias voltage, CF_4 contents and input power [17]. In this study, the influence of the burst width on the electric and etching characteristics was investigated. The etching was performed on samples placed in the bulk plasma. The electrical characteristics were evaluated by time-resolved measurements. The burst width was varied in the range of 400–1000 µs. The target current and etching rate were evaluated at each burst width.

2. Experimental Procedure

Figure 1 shows a schematic of the experimental apparatus. The vacuum chamber consisted of a cylindrical glass tube (51 mm inner diameter, 55 mm external dimeter). The plasma source consisted of a solenoid coil (50 turns, length 70 mm, 83.7 µH) wound on a glass tube. A capacitor (12 nF) was connected to the coil in parallel and was used to build a resonance circuit with the coil. The capacitance and inductance were resonant with a frequency of about 157 kHz. The 400–1000 µs wide high voltage burst pulses with a frequency of 157 kHz were generated using a power supply (PS-1, PEKURIS KJ14-4873, Kyoto, Japan) and applied to the solenoid coil to generate ICP. The number of sine waves per burst pulse was 157 for the burst width of 1ms, and the repetition rate of the burst pulse was 10 Hz. Argon and tetrafluoro-carbon gases were supplied through mass flow controllers (SEC-400MK3 and SEC-E40MK3, HORIBA, Kyoto, Japan) into the chamber. Total gas flow rate was controlled in range of 19.3–41.7 sccm. The solenoid coil voltage and current were measured by a high voltage probe (P6015A, Tektronix, Beaverton, OR, USA) and a current monitor (model 110A, Pearson, London, UK), respectively.

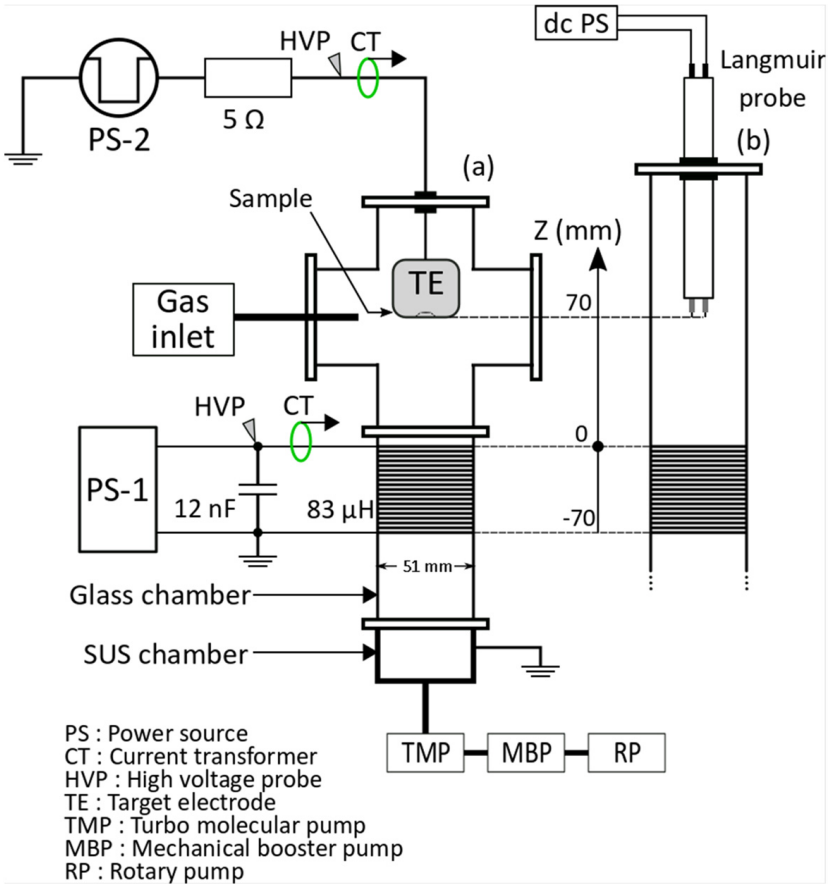

Figure 1. Schematic of the experimental apparatus.

Figure 2 shows the structure of the target electrode used in the etching process. The silicon wafer to be etched ((100), 12.6 mm diameter, 250 μm thickness) was set on the target electrode. A stainless steel mask (12.6 mm diameter, 150 μm thickness) with 1 mm square holes was placed on the wafer. The target electrode was made of titanium (26 mm diameter, 35 mm length) and had a cylindrical shape. The target electrode was placed inside the chamber. The distance between the target electrode and the end of the coil was 70 mm as shown in Figure 1. A negative-polarity rectangular pulse voltage with a pulse width of 1000 μs and a voltage of 800 V was applied to the target electrode by a power supply (PS-2, PEKURUS KJ06-3265, Kyoto, Japan) via a current limiting resistor of 5 Ω consisting of two 10 Ω resistors connected in parallel. The repetition rate was set to 10 Hz and the application timing was synchronized with the burst signal. During the first 4 min of etching, the presputter process was done by gradually increasing the bias voltage from about −100 V. The specified bias voltage was applied to the target for 20 min after the presputter process. After etching process, the etching depth of the wafer was measured by a surface roughness tester (Form Talysurf Super S5K, Taylor Hobson, Leicester, UK), and the etching rate was calculated by dividing the etching depth by the processing time [17]. The voltage applied to the target and current flowing through the electrodes were measured by a high voltage probe (P-5100, Tektronix) and current monitor (model 110A, Pearson), respectively.

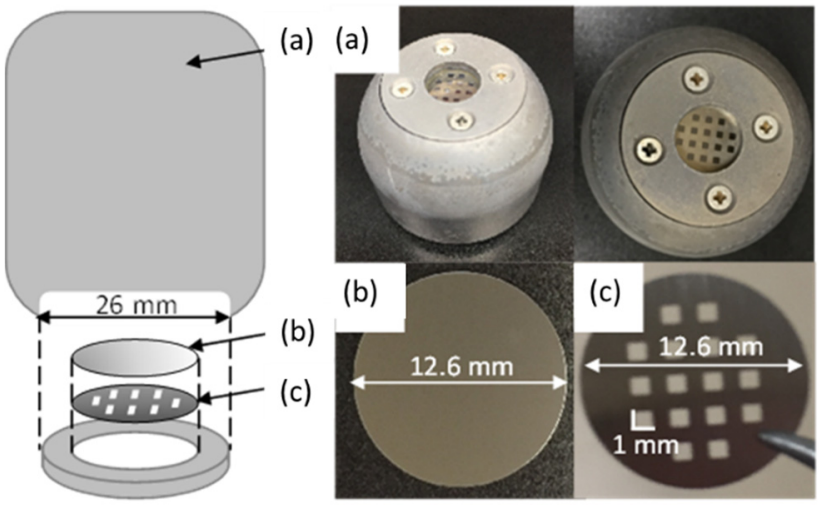

Figure 2. Structure of target electrode. (**a**) Target electrode, (**b**) silicon wafer, and (**c**) stainless steel mask.

The electron temperature and the ion density were obtained by floating double probe measurements [20–23]. The probe tip was a cylindrical tungsten electrode (ϕ 0.4) with an exposed length of 3 mm and a tip-to-tip distance of 8 mm. The measurement position of the probe was 70 mm from the coil edge. Electron energy distribution function was assumed as Maxwellian 2 [14,24].

3. Results and Discussion

Figure 3 shows the typical waveforms of the coil voltage and coil current, and the time evolution of the effective electrical power, the power factor, the impedance, the resistance and the reactance for pure Ar discharge and Ar/CF_4 discharge. The total flow rates in Ar and Ar/CF_4 discharge were Ar = 41.7 sccm and Ar/CF_4 = 35.4/6 sccm, respectively, and the CF_4 content rate was 15%. The pressure was 5 Pa. The burst width was 1000 μs and the repetition rate was 10 Hz. The duty ratio was 1%. The waveform was divided into 3 stages (I)~(III) as shown in Figure 3. The ICP in Ar/CF_4 discharge was ignited at 40 μs (stage (II)). The peak values of coil voltage and current before the ICP ignition (stage (I)) were approximately 3.4 kV and 39 A, respectively. The impedance calculated from the amplitude of the coil voltage and current was about 87 Ω, which was almost equal

to the impedance of the induction coil of 83 Ω. After the plasma ignition (stage (III)), the coil voltage and current decreased to 1.7 kV and 21 A, respectively. When the plasma was generated, a transformer, where the plasma was regarded as the secondary winding was coupled between the coil and the plasma, and the impedance changed. The impedance at this time was approximately 81 Ω [25,26]. After the time of 400 µs (stage (III)), the coil voltage and current increased again to approximately 2.2 kV and 25 A, respectively. This trend of time evolution was also observed in the Ar discharge. The amplitudes of the coil voltage and current were slightly larger when CF_4 was included. When CF_4 was added, the electron density decreased by electron attachment, and the plasma resistance, which was determined by collusions between electrons and other particles, was reduced. The power factor after the plasma generated was approximately 20%, and the effective power of the coil was approximately 4.5 kW. Therefore, the average power was 45 W at a repetition rate of 10 Hz.

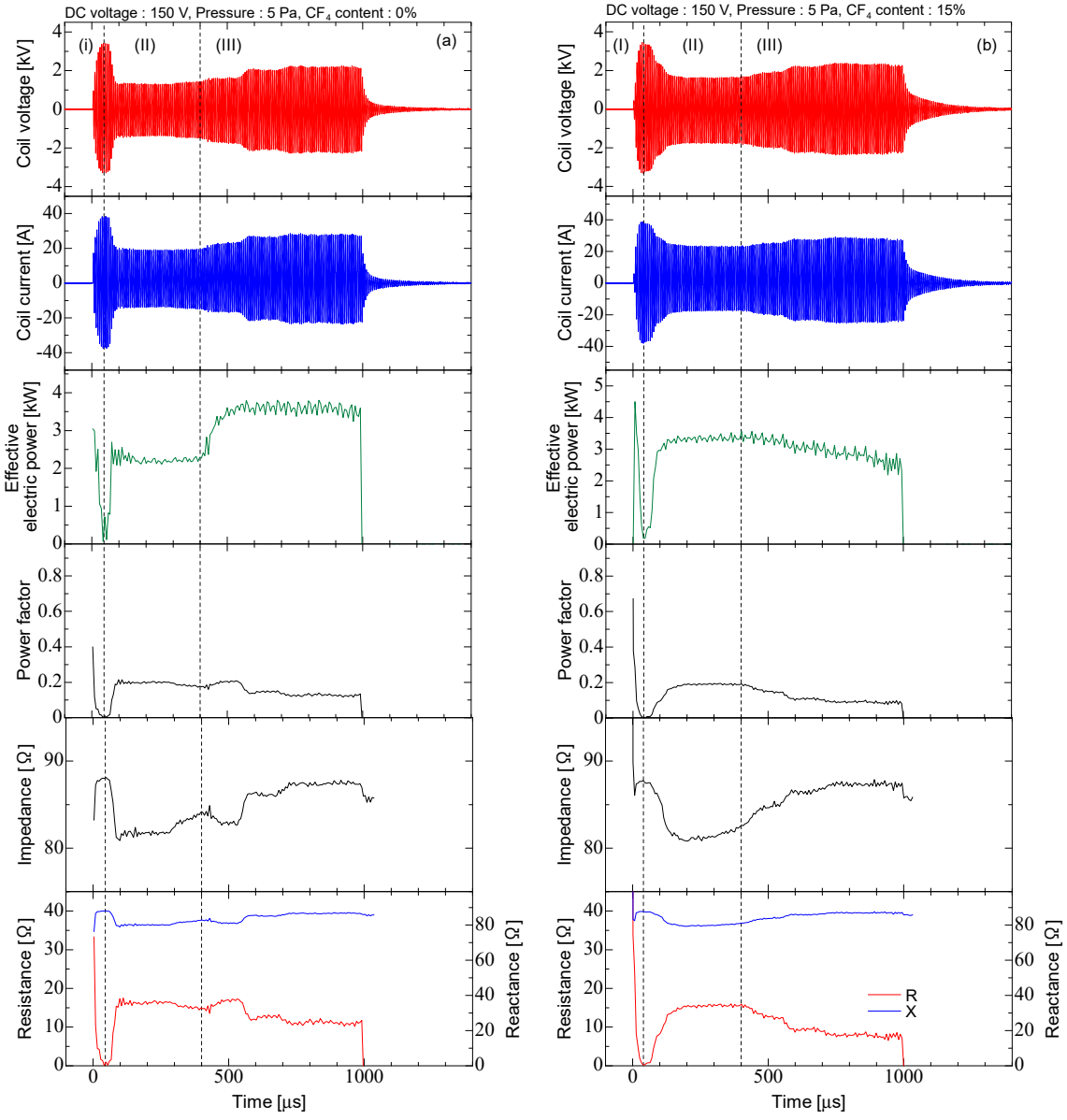

Figure 3. Typical waveforms of the coil voltage, coil current, the time evolution of the effective electrical power, the power factor, the impedance, the resistance and the reactance. (**a**) Ar discharge and (**b**) Ar/CF_4 discharge (**I**) before discharge, (**II**) constant discharge, (**II**) discharge.

The effective electrical power and the power factor for Ar and Ar/CF_4 discharges were obtained by waveforms of coil voltage and current. The power factor was obtained from the phase difference at zero-cross timing between the voltage and current. In the Ar discharge, approximately 2 kW of power was consumed between 200–400 μs (32–63 cycle) in stage (II). After that, it increased to approximately 3.5 kW, and then became constant after 600 μs (90 cycle) in stage (III). The power factor increased rapidly from 0.0010 to 0.20 between 40–100 μs (6–6 cycles) in stage (I). After that, it gradually decreased to 0.21 in stage (II), and then decreases to 0.13, and then has a constant value in stage (III). In the Ar/CF_4 discharge, approximately 3 kW of power was consumed during the discharge. The power factor increased rapidly from 0.0029 to 0.16 between 40–130 μs (6–20 cycles) in stage (I). After that, it gradually increased to 0.19 at 200 μs (32 cycle), and then decreased to 0.10 at 580 μs (94 cycle). After that, it was almost constant in stage (III).

In the Ar discharge, the impedance decreased rapidly from 88.0 Ω to 80.9 Ω between 40–110 μs (6–16 cycle) in stage (I), and it increased to 84.1 Ω in stage (II). After that, it decreased again to 82.7 Ω at 530 μs (80 cycle), and it increased gradually to 87.4 Ω in stage (III). This trend of time evolution was also observed in the resistance and the reactance. The resistance had a symmetrical trend, and the reactance had the same trend as the impedance. In the Ar/CF_4 discharge, the impedance decreased rapidly from 87.8 Ω to 82.3 Ω between 40–130 μs (6–19 cycle) in stage (I), and it decreased to 80.8 Ω in stage (II). After that, the impedance gradually increased to 87.1 Ω in stage (III). The impedance change had the same timing as the coil voltage and current. The resistance increased rapidly from 0.25 Ω to 13.1 Ω between 40–130 μs in stage (I). The resistance increased in the number of electron collisions with other particles in the plasma [26–30]. Thus, the electron density increased rapidly during this period. After that, it increased slightly to 15.2 Ω, and it was almost constant until 400 μs in stage (II). After 400 μs, the resistance component decreased at 600 μs in stage (III). The loss process of electrons was larger than the generation of electrons in this period. After 600μs, the resistance was almost constant. The reactance change timing was the same as that of the resistance. Because the reactance decreased between 40–130 μs, and it increased until 600 μs, and it was almost constant.

Figure 4 shows the effective values of the coil voltage and current for Ar discharge, Ar/CF_4 discharge, effective power and power factor as a function of input power. The input power was the time average of the power to the coil during the discharge. The coil voltage and current increased with the input power. The values of coil voltage and current in Ar and Ar/CF_4 discharges were almost equal. The effective power was almost equal for Ar and Ar/CF_4 discharges, ranging from about 3.0–11 kW. It was found that it increased linearly with the input power. The power factor increased with input power and it was 0.19–0.28. The power factor in Ar/CF_4 discharge was smaller than the Ar discharge.

Figure 5 shows the impedance (Z), resistance (R), and reactance (X) during the discharge as functions of the input power. The impedance decreased with increasing input power. The impedance of Ar/CF_4 discharge was larger than that of the Ar discharge. The resistance increased, and the reactance decreased with increasing input power. The resistance during discharge was 15–21 Ω for Ar discharge and 15–20 Ω for Ar/CF_4 discharge, which was larger than the parasitic resistance of the coil, 0.16 Ω. The reactance of the Ar/CF_4 discharge was higher than that of the Ar discharge.

Figure 6 shows the electron temperature (T_e) and plasma density (n_p) of Ar and Ar/CF_4 discharges as functions of the input power. The target electrode was not placed in the chamber. The probe measurement position was 70 mm from the coil edge. The ion density n_i is obtained as following equation [31],

$$n_i = J/0.61eu_B \quad (1)$$

where J is the target current density obtained from the measured target current I_t, u_B is Bohm velocity and e is an elementary charge. The electron temperature is 2–3 eV and is not affected by gas species. In conventional ICP, the electron temperature is around 3.5 eV [9,32–34], and this ICP is almost equal to the conventional value. The plasma density

increases with the input power, and is on the orders of 10^{19} m^{-3} in Ar discharge, and 10^{18} m^{-3} in Ar/CF_4 discharge. In conventional ICP, the plasma density is on the orders of 10^{17}–10^{18} m^{-3} in Ar discharge, and 10^{16} m^{-3} in Ar/CF_4 discharge [1,5,35]. In this ICP, it was 10 to 100 times higher than the conventional ICP. Therefore, it is expected to be applied to high-speed processes. The plasma density in the Ar/CF_4 discharge is lower than that in Ar discharge because of electron loss due to electron attachment to various kinds of molecules [35–38]. When an electronegative gas such as CF_4 is fed into the chamber, the potential structure in the sheath has two-stages. In this case, the negative ions are confined to the center of the plasma, and the positive ion current flowing through the electrode is proportional to the electron density, not to the positive ions. Therefore, the value of the obtained saturated ion current is different from that for positive ions only. Assuming that only a single negative ion species is presented in the plasma, and it is lost by the recombination with positive ions, the balance equation can be expressed as follows,

$$k_a n_e N_0 = k_r N_p N_n \approx k_r N_n^2 \quad (2)$$

where k_a is the attachment rate coefficient, k_r is the recombination coefficient, n_e is electron density, N_p is positive ion density, N_n is negative ion density, and N_0 is the reaction gas density (in this case, CF_4 density). From the quasi-neutral condition with $n_p \approx n_n$, the ratio of the negative ion density t the electron density, β, in Equation (2) becomes,

$$\beta = \sqrt{k_a N_0 / k_r n_e} \quad (3)$$

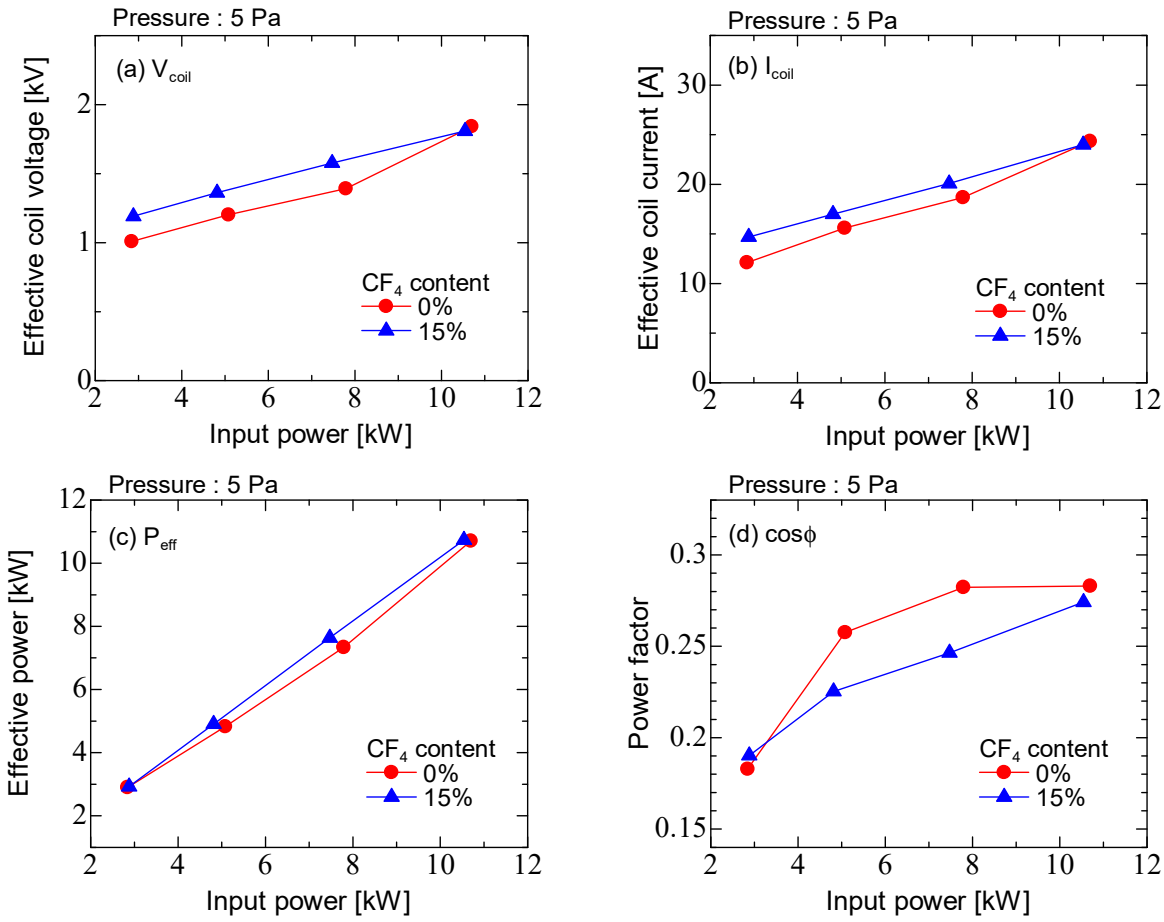

Figure 4. Electrical characteristics of the ICP as a function of input power for Ar discharge and Ar/CF_4 discharge. (**a**) Effective coil voltage, (**b**) effective coil current, (**c**) effective power and (**d**) power factor.

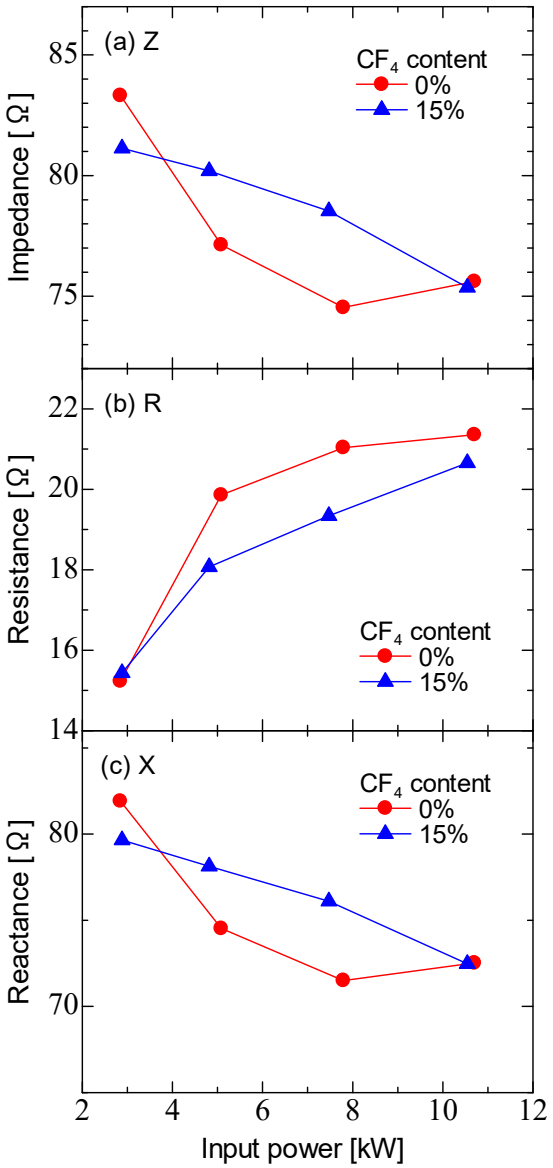

Figure 5. Electrical characteristics of the ICP as a function of input power for Ar discharge and Ar/CF_4 discharge. (**a**) impedance, (**b**) resistance and (**c**) reactance.

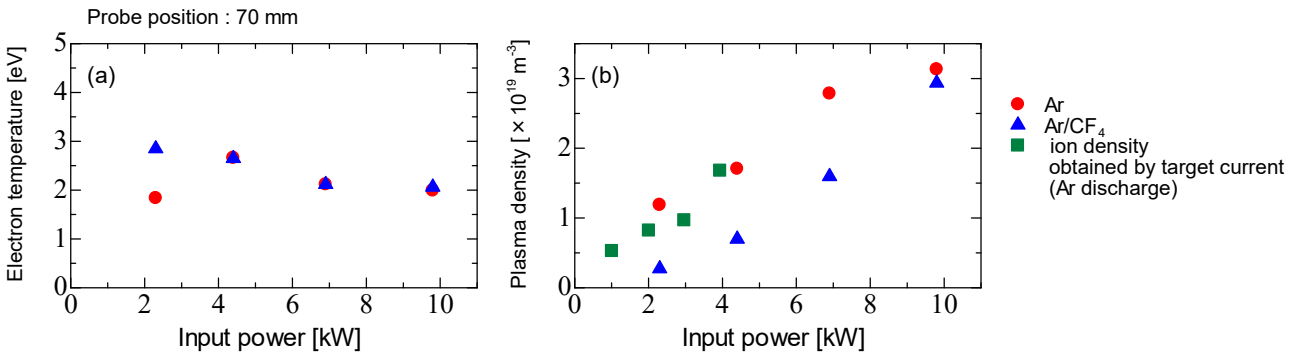

Figure 6. Plasma parameters as a function of input power. (**a**) Electron temperature and (**b**) plasma density for Ar and Ar/CF_4 discharges.

Assuming the negative ion is only F^- and the electron temperature is 3 eV, k_a, k_r and β are estimated as 8.9×10^{-17} m^3s^{-1}, 4.0×10^{-13} m^3s^{-1}, and 0.065, respectively [36,37,39]. Therefore, the negative ion density is 7.15×10^{17} m^{-3}. Because the negative ion density is much smaller than the electron density, the negative ion does not affect the saturated ion current flowing into the probe.

Figure 7 shows the target current for Ar discharge and Ar/CF_4 discharge for each burst width at a pressure of 5 Pa. The target position was 70 mm from the coil edge. The bias voltage was −800 V, and the pulse width was synchronized with the burst width. In the Ar discharge with a burst width of 1000 µs, the target current rose from approximately 130 µs. The target current reached a maximum value of about 2.5 A at 600 µs. The voltage drop across the current control resistor (5 Ω) was a few tens of volts and was sufficiently low to the bias voltage. In the Ar/CF_4 discharge, the target current gradually rose from approximately about 150 µs and reached a maximum value of approximately 1.1 A at 650 µs. The maximum current value was approximately half of that of the Ar discharge. The target current decreased significantly and the current rise time was delayed when the CF_4 was fed in. Because CF_4 was fed into the chamber, the ion density decreased and the target current decreased. The burst width increased, the maximum value of the target current became slightly larger, and the rise time became shorter. The density of high-energy electrons increased with burst width.

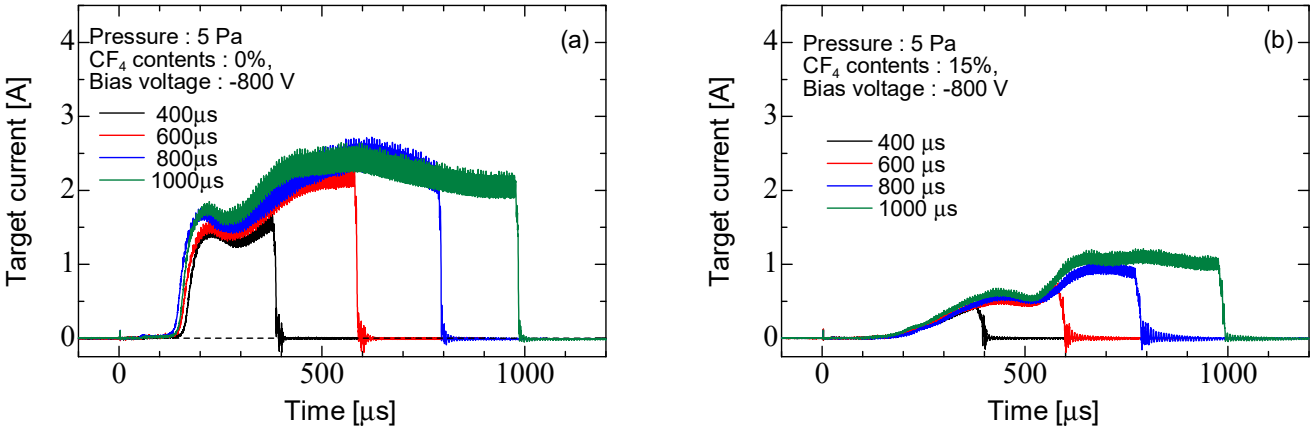

Figure 7. Waveform of target current at each burst width (**a**) Ar discharge and (**b**) Ar/CF_4 discharge.

Figure 8 shows the target current for Ar discharge and Ar/CF_4 discharge at each input power. Ar = 19.3 sccm, Ar/CF_4 = 14.4/5 sccm, for the pressure of 3 Pa. The burst width was 400 µs, the repetition rate was 25 Hz, and duty rate was 1%. The target position was 70 mm from the coil edge. The bias voltage was −800 V, and the pulse width was synchronized with the burst width. The burst width was set to 400 µs in order to reduce the arcing at the target electrode and make the process stable. The pressure was changed from 5 to 3 Pa by reducing the gas flow rate from 41.7 to 19.3 sccm also, in order to inhibit the arcing. As noted in Figure 9, the density of the Ar discharge was of the order of 10^{19} m^{-3} and the Ar/CF_4 discharge was of the order of 10^{18} m^{-3}. The input power increased, the maximum value of the target current became larger, and the time to ignite plasma and the rise time of the target current became shorter. The high-energy electrons increased with input power, which accelerated the ionization. When CF_4 was added, the EEDF showed a decrease in the fraction of low-energy electrons and an increase in the fraction of high-energy electrons [36,38]. This suggests that the generation process of Ar ions is dominated by the multistep ionization of Ar atoms in the Ar discharge, and direct ionization from the ground state increases in Ar/CF_4 discharge. Therefore, the discharge is ignited earlier by the addition of CF_4. In addition, a large change in the target current was observed at 3.0 kW and 3.9 kW in the Ar discharge. As shown in Figure 6, the plasma density in Ar/CF_4 discharge was smaller than the Ar discharge at low input power, because the attachment

rate of electrons in CF_4 is larger than the ionization rate in Ar at low input power, i.e., a low reduced electric field (E/N) [10]. Therefore, the plasma density decreases with adding CF_4 gas into Ar gas at low input power. However, the ionization rate in Ar is much larger than the attachment rate of electrons in CF_4 at high input power, i.e., a high reduced electric field (E/N) [10]. Therefore, the plasma density in the Ar/CF_4 discharge had almost same value as that in the Ar discharge at high input power, as shown in Figure 6b. The plasma impedance is affected by the plasma density. The change of plasma impedance is one of the reasons for the target current fluctuation shown in Figure 8. However, more study is needed to clarify the detail of the mechanism.

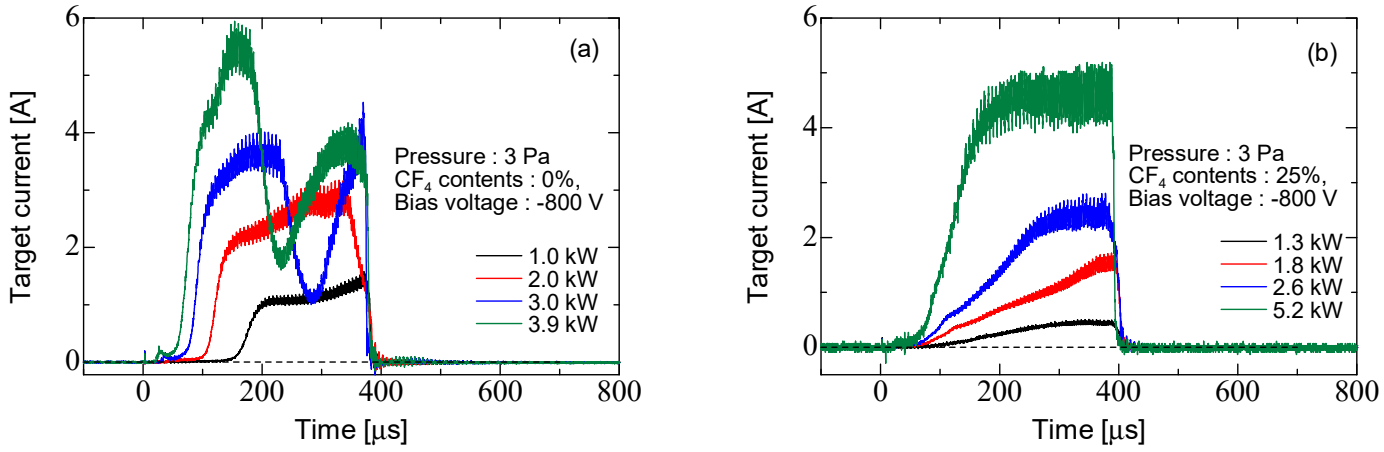

Figure 8. Waveform of target current at each input power. (**a**) Ar discharge and (**b**) Ar/CF_4 discharge.

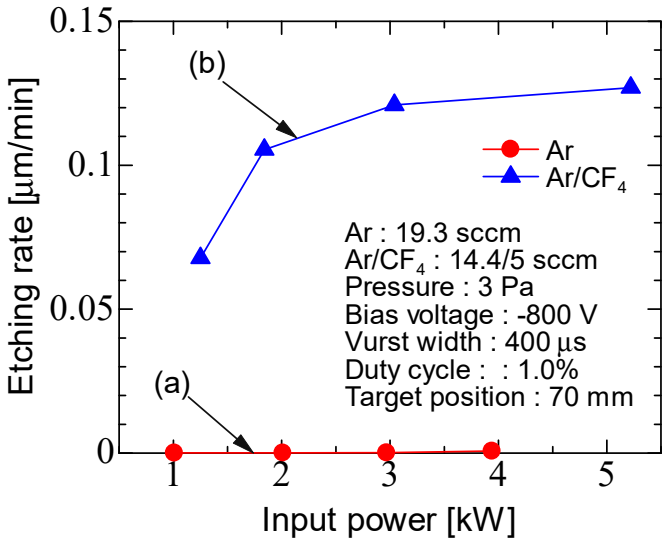

Figure 9. Input power characteristics of the etching rate for (**a**) Ar discharge and (**b**) Ar/CF_4 discharge.

Figure 9 shows the etching rate for Ar discharge and Ar/CF_4 discharge as a function of the input power. The etching rate by Ar discharge was much smaller than Ar/CF_4 discharge. Because in the etching in Ar discharge, the Ti target electrode was etched by argon ions, and fractions were deposited in the trench [17]. The etching rate in Ar/CF_4 discharge increased with input power, and the maximum etching rate was 0.13 μm/min. In conventional ICP, the etching rate is 0.02–0.03 μm/min [40]. In this ICP, the etching rate was faster than the conventional ICP. This is supported by the high density compared to the conventional ICP.

Figure 10 shows the etching rate for Ar discharge and Ar/CF_4 discharge as a function of the burst width with a repetition rate of 10 Hz. The repetition rate was fixed, the input power per cycle was increased with burst width. Ar = 41.7 sccm, Ar/CF_4 = 35.4/6 sccm, and the pressure was 5 Pa. In Ar discharge, the etching rate increased slightly with the increasing burst width and was about 0.005 μm/min. In Ar/CF_4 discharge, the etching rate increased slightly with the increasing burst width and was about 0.02–0.05 μm/min. The etching rate in the case of Ar/CF_4 discharge was 4–10 times higher than that of Ar discharge.

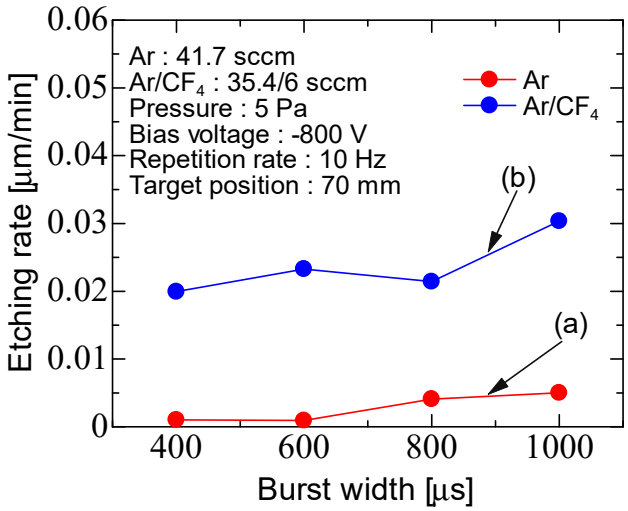

Figure 10. Burst width characteristics of the etching rate for (**a**) Ar discharge and (**b**) Ar/CF_4 discharge with fixed repetition rate (10 Hz).

Figure 11 shows the etching rate for Ar discharge and Ar/CF_4 discharge as a function of the burst width with a duty cycle of 1.2%. The duty cycle was fixed, the input power per cycle did not change. When the duty ratio was fixed, there was no significant change with the burst width, unlike when the repetition rate was fixed. Therefore, the etching rate is affected by the input power. The etching rate was about 0.005 μm/min for Ar discharge and 0.04–0.05 μm/min for Ar/CF_4 discharge.

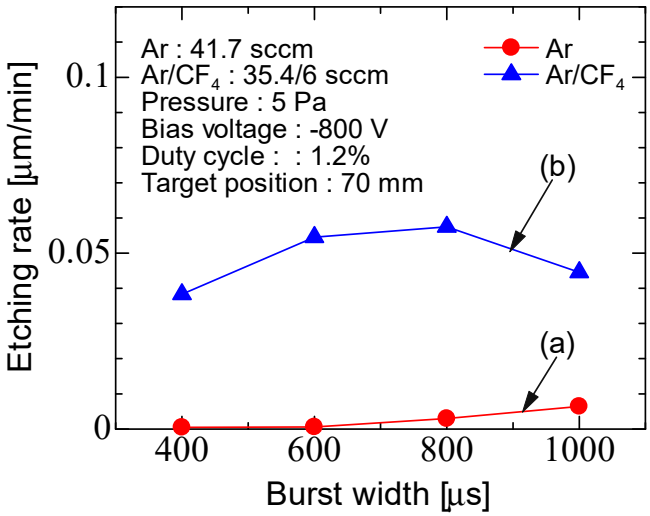

Figure 11. Burst width characteristics of the etching rate for (**a**) Ar discharge and (**b**) Ar/CF_4 discharge with fixed duty cycle (1.2%).

4. Conclusions

The electrical characteristics and etching rates of the high-power burst Ar and Ar/CF_4 ICPs were investigated. The effective power, power factor and impedance were obtained by time-resolved measurements. The etching was operated in Ar and Ar/CF_4 discharges, and the effects of the power and burst width were investigated. It was found that during Ar/CF_4 discharge, about 3 kW was applied. It was confirmed that the coil current and voltage changed with the impedance. The power factor in Ar/CF_4 discharge was slightly smaller than Ar discharge, and the impedance was larger than the Ar discharge. Double probe measurements showed that the plasma density in the etching area was in the order of 10^{18}–10^{19} m^{-3}, that the etching was performed under high density. The etching rate of the silicon wafer by Ar/CF_4 discharge (reactive ion etching) was larger than the Ar discharge (physical etching) and increased 0.05 μm/min with the burst width increasing at a constant repetition rate. At this time, since the duty ratio is 1.0%, a DC equivalent value of 5 μm/min could be obtained.

Author Contributions: H.K., K.T. (Katsuyuki Takahashi), S.M., K.T. (Koichi Takaki), and K.Y. conceived and designed the experiments; H.K. performed the experiments; H.K. and K.T. (Koichi Takaki) analyzed the data; H.K., K.T. (Katsuyuki Takahashi) and K.T. (Koichi Takaki) wrote the paper. All authors have read and agreed to the published version of the manuscript.

Funding: This research was supported by a Grant-in-Aid for Scientific Research (S) from the Japan Society for the Promotion of Science, Grant Number 19H05611.

Acknowledgments: The author would like to thank K.Y. for his valuable comments and discussions. The author would also like to thank Yutaka Shida at the Iwate University technical staff.

Conflicts of Interest: The authors declare no conflict of interest.

References

1. Helmersson, U.; Lattemann, M.; Bohlmark, J.; Ehiasarian, A.P.; Gudmundsson, J.T. Ionized physical vapor deposition (IPVD): A review of technology and applications. *Thin Solid Films* **2006**, *513*, 1–24. [CrossRef]
2. Donnelly, V.M.; Kornblit, A. Plasma etching: Yesterday, today, and tomorrow. *J. Vac. Sci. Technol.* **2013**, *31*, 050825. [CrossRef]
3. Hopwood, J. Ionized physical vapor deposition of integrated circuit interconnects. *Phys. Plasma* **1998**, *5*, 1624–1631. [CrossRef]
4. Koyanagi, M.; Kurino, H.; Lee, K.W.; Sakuma, K.; Miyakawa, N.; Itani, H. Future System-on-Silicon LSI Chips. *IEEE Micro.* **1998**, *18*, 17–22. [CrossRef]
5. Hopwood, J.; Search, H.; Journals, C.; Contact, A.; Iopscience, M.; Sci, P.S.; Address, I.P. Review of inductively coupled. *Plasma Sources Sci. Technol.* **1992**, *1*, 109–116. [CrossRef]
6. Xu, S.; Ostrikov, K.N.; Li, Y.; Tsakadze, E.L.; Jones, I.R. Low-frequency, high-density, inductively coupled plasma sources: Operation and applications. *Phys. Plasmas* **2001**, *8*, 2549–2557. [CrossRef]
7. Teske, C.J.; Jacoby, J. Pulsed low frequency inductively coupled plasma generator and applications. *IEEE Trans. Plasma Sci.* **2008**, *36*, 1930–1936. [CrossRef]
8. Guo, W.; DeJoseph, C.A. Time-resolved current and voltage measurements on a pulsed rf inductively coupled plasma. *Plasma Sources Sci. Technol.* **2001**, *10*, 43–51. [CrossRef]
9. Lieberman, M.A.; Lichtenberg, A.J. *Principles of Plasma Discharges and Materials Processing*, 2nd ed.; Wiley: New York, NY, USA, 2005.
10. Makabe, T.; Petrovic, Z.L. *Plasma electronics: Applications in Microelectronic Device Fabrication*, 2nd ed.; CRC Press: New York, NY, USA, 2014.
11. Tuszewski, M.; Scheuer, J.T.; Adler, R.A. A pulsed inductively coupled plasma source for plasma-based ion implantation. *Surf. Coat. Technol.* **1997**, *93*, 203–208. [CrossRef]
12. Yukimura, K.; Ehiasarian, A.P. Generation of RF plasma assisted high power pulsed sputtering glow discharge without using a magnetic field. *Nucl. Instrum. Methods Phys. Res. B* **2009**, *267*, 1701–1704. [CrossRef]
13. Yukirnnra, K.; Ogiso, H.; Nakano, S.; Ehiasarian, A.P. High-power inductively coupled impulse sputtering glow plasma. *IEEE Trans. Plasma Sci.* **2011**, *39*, 3085–3093.
14. Yukimura, K.; Ogiso, H.; Nakano, S. Ionization of sputtered carbon species by high-power inductively-coupled impulse sputtering (ICIS). *Vacuum* **2018**, *153*, 195–203. [CrossRef]
15. Shibata, K.; Konno, S.; Takahashi, K.; Mukaigawa, S.; Takaki, K.; Yukimura, K. Electrical and plasma characteristics of 150 kHz band high-power burst inductively coupled plasma. In Proceedings of the 2017 IEEE 21st International Conference on Pulsed Power, Brighton, UK, 18–22 June 2017.

16. Saito, Y.; Shibata, K.; Takahashi, K.; Mukaigawa, S.; Takaki, K.; Yukimura, K. Global model analysis of Ar inductively coupled plasma driven by a 150 kHz-band high-power pulse burst. *Jpn. J. Appl. Phys.* **2019**, *58*, SAAB06. [CrossRef]
17. Saito, Y.; Shibata, K.; Takahashi, K.; Mukaigawa, S.; Takaki, K.; Yukimura, K.; Ogiso, H.; Nakano, S. Silicon wafer etching by pulsed high-power inductively coupled Ar/CF_4 plasma with 150 kHz band frequency. *Jpn. J. Appl. Phys.* **2020**, *59*, SHHE04. [CrossRef]
18. Hara, S.; Maekawa, S.; Ikeda, S.; Nakano, S. Concept of minimal fab and development of minimal equipments. *J. Jpn. Soc. Precis. Eng.* **2011**, *77*, 249–253. [CrossRef]
19. Yukimura, K.; Ogiso, H.; Nakano, S. Film deposition using 1-inch-sized HIPIMS system-Toward minimal fabrication semiconductor poduction system. *Surf. Coat. Technol.* **2014**, *250*, 26–31. [CrossRef]
20. Johnson, E.O.; Malter, L. A floating double probe method for measurments in gas discharges. *Phys. Rev.* **1950**, *80*, 58–70. [CrossRef]
21. Demidov, V.I.; Ratynskaia, S.V.; Rypdal, K. Electric probes for plasmas: The link between theory and instrument. *Rev. Sci. Instrum.* **2002**, *73*, 3409–3439. [CrossRef]
22. Cherrington, B.E. The use of electrostatic probes for plasma diagnostics-A review. *Plasma Chem. Plasma Process.* **1982**, *2*, 113–140. [CrossRef]
23. Yin, Y.; Messier, J.; Hopwood, J.A. Miniaturization of inductively coupled plasma sources. *IEEE Trans. Plasma Sci.* **1999**, *27*, 1516–1524. [CrossRef]
24. Kimura, T.; Ohe, K. Electron energy distribution detection in symmetrically driven rf argon discharge. *Jpn. J. Appl. Phys.* **1993**, *32*, 3601–3605. [CrossRef]
25. Piejak, R.B.; Godyak, V.A.; Alexandrovich, B.M. A simple analysis of an inductive RF discharge. *Plasma Sources Sci. Technol.* **1992**, *1*, 179–186. [CrossRef]
26. Gudmundsson, J.T.; Lieberman, M.A. Magnetic induction and plasma impedance in a cylindrical inductive discharge. *Plasma Sources Sci. Technol.* **1997**, *6*, 540–550. [CrossRef]
27. Chang, C.H.; Leou, K.C.; Chen, C.H.; Lin, C. Measurements of time resolved rf impedance of a pulsed inductively coupled Ar plasma. *Plasma Sources Sci. Technol.* **2006**, *15*, 338–344. [CrossRef]
28. Cunge, G.; Crowley, B.; Vender, D.; Turner, M.M. Characterization of the E to H transition in a pulsed inductively coupled plasma discharge with internal coil geometry: Bi-stability and hysteresis. *Plasma Sources Sci. Technol.* **1999**, *8*, 576–586. [CrossRef]
29. Yang, J.G.; Yoon, N.S.; Kirn, B.C.; Choi, J.H.; Lee, G.S.; Hwang, S.M. Power absorption characteristics of an inductively coupled plasma discharge. *IEEE Trans. Plasma Sci.* **1999**, *27*, 676–681. [CrossRef]
30. Kortshagen, U.; Gibson, N.D.; Lawler, J.E. On the E-H mode transition in RF inductive discharges. *J. Phys. D Appl. Phys.* **1996**, *29*, 1224–1236. [CrossRef]
31. Abe, S.; Takahashi, K.; Mukaigawa, S.; Takaki, K.; Yukimura, K. Comparison of plasma characteristics of high-power pulsed sputtering glow discharge and hollow-cathode discharge. *Jpn. J. Appl. Phys.* **2020**, *60*, 015501. [CrossRef]
32. Hopwood, J.; Guarnieri, C.R.; Whitehair, S.J.; Cuomo, J.J. Electromagnetic fields in a radio-frequency induction plasma. *J. Vac. Sci. Technol.* **1993**, *11*, 147–151. [CrossRef]
33. Haas, F.A.; Braithwaite, N.S.J. Tailoring of electron energy distributions in low-pressure inductive discharges. *Appl. Phys. Letteers* **1999**, *74*, 338–340. [CrossRef]
34. Palmero, A.; Van Hattum, E.D.; Rudolph, H.; Habraken, F.H.P.M. Characterization of a low-pressure argon plasma using optical emission spectroscopy and a global model. *J. Appl. Phys.* **2007**, *101*, 053306. [CrossRef]
35. Efremov, A.M.; Kim, D.P.; Kim, K.T.; Kim, C.I. Etching characteristics and mechanism of Pb(Zr,Ti)O_3 thin films in CF_4/Ar inductively coupled plasma. *Vacuum* **2004**, *75*, 321–329. [CrossRef]
36. Kimura, T.; Ohe, K. Probe measurements and global model of inductively coupled Ar/CF_4 discharge. *Plasma Sources Sci. Technol.* **1999**, *8*, 553–560. [CrossRef]
37. Efremov, A.M.; Kim, D.P.; Kim, C.I. Effect of gas mixing ratio on gas-phase composition and etch rate in an inductively coupled CF_4/Ar plasma. *Vacuum* **2004**, *75*, 133–142. [CrossRef]
38. Zhao, S.X.; Gao, F.; Wang, Y.N.; Bogaerts, A. The effect of F 2 attachment by low-energy electrons on the electron behaviour in an Ar/CF 4 inductively coupled plasma. *Plasma Sources Sci. Technol.* **2012**, *21*, 025008. [CrossRef]
39. Christophorou, L.G.; Olthoff, J.K.; Rao, M.V.V.S. Electron interactions with CF_4. *J. Phys. Chem. Ref. Data* **1996**, *25*, 1341–1388. [CrossRef]
40. Kumar, A.; Lee, W.H.; Wang, Y.L. Optimizing the isotropic etching nature and etch profile of Si, Ge and Si0.8Ge0.2 by controlling CF4 atmosphere with Ar and O2 additives in ICP. *IEEE Trans. Semicond. Manuf.* **2021**, *34*, 177–184. [CrossRef]